



Deposited via The University of Leeds.

White Rose Research Online URL for this paper:

<https://eprints.whiterose.ac.uk/id/eprint/96296/>

Version: Accepted Version

Article:

Walter, S, Bollenbach, A, Doerrbecker, J et al. (2016) Ion-channel function and cross-species determinants in viral assembly of nonprimate hepacivirus p7. *Journal of Virology*, 90 (10). pp. 5075-5089. ISSN: 0022-538X

<https://doi.org/10.1128/JVI.00132-16>

Reuse

Items deposited in White Rose Research Online are protected by copyright, with all rights reserved unless indicated otherwise. They may be downloaded and/or printed for private study, or other acts as permitted by national copyright laws. The publisher or other rights holders may allow further reproduction and re-use of the full text version. This is indicated by the licence information on the White Rose Research Online record for the item.

Takedown

If you consider content in White Rose Research Online to be in breach of UK law, please notify us by emailing eprints@whiterose.ac.uk including the URL of the record and the reason for the withdrawal request.

23

24 **Running title:** Determinants of nonprimate hepacivirus p7 for ion-channel activity and virus
25 assembly

26 **Keywords:** hepatitis C virus, p7, nonprimate hepacivirus, equine hepacivirus, ion-channel

27

28 Word count, abstract: 250

29 Word count, text: 6376

30

31 ***Contact Information**

32 PD Dr. Eike Steinmann

33 Institute for Experimental Virology

34 TWINCORE, Centre for Experimental and Clinical Infection Research; a joint venture between
35 the Medical School Hannover (MHH) and the Helmholtz Centre for Infection Research (HZI)

36 Feodor-Lynen-Str. 7, 30625 Hannover, Germany

37 Phone: +49 511 2200 27134 Fax: +49 511 2200 27139

38 E-mail: Eike.Steinmann@twincore.de

39

40

41 **Abbreviations**

42 CF: carboxyfluorescein

43 DAA: direct acting antiviral

44 EI-IRES: encephalomyocarditis virus internal ribosomal entry site

45 ER: endoplasmic reticulum

- 46 FU: fluorescent units
- 47 G-Luc: *Gaussia*-Luciferase
- 48 GBV-B: GB virus B
- 49 GT: genotype
- 50 HCV: hepatitis C virus
- 51 HCVcc: HCV cell culture derived particles
- 52 MAVS: mitochondrial antiviral signaling protein
- 53 MD: molecular dynamics
- 54 NMR: nuclear magnetic resonance spectroscopy
- 55 MN-DGJ: *N*-nonyl-deoxygalactonojirimycin
- 56 MN-DNJ: *N*-nonyl-deoxynojirimycin
- 57 NPHV: nonprimate hepacivirus
- 58 ORF: open reading frame
- 59 PI-IRES: poliovirus internal ribosomal entry site
- 60 RT: room temperature
- 61 SP: signal peptide
- 62 TM1/2: transmembrane helix 1/2
- 63 TRIF: Toll-IL-1 receptor domain-containing adaptor inducing interferon-beta
- 64 UTR: untranslated regions
- 65

66 **Abstract**

67 Nonprimate hepacivirus (NPHV), the closest homolog of hepatitis C virus (HCV) described to
68 date, has recently been discovered in horses. Even though both viruses share a similar genomic
69 organization, conservation of the encoded hepaciviral proteins remains undetermined. The HCV
70 p7 protein is localized within endoplasmic reticulum (ER) membranes and is important for
71 production of infectious particles. In this study, we analyzed the structural and functional features
72 of NPHV p7 in addition to its role during virus assembly. Three-dimensional homology models
73 for NPHV p7 by using various NMR structures were generated highlighting conserved residues
74 important for ion-channel function. By applying a liposome permeability assay, we observed that
75 NPHV p7 exhibited similar liposome permeability features than HCV p7 indicative of similar
76 ion-channel activity. Next, we characterized the viral protein using a p7-based *trans*-
77 complementation approach. A similar sub-cellular localization pattern at the ER membrane was
78 observed, although production of infectious particles was likely hindered by genetic
79 incompatibilities with HCV proteins. To further characterize these cross-species constraints,
80 chimeric viruses were constructed by substituting different regions of HCV p7 with NPHV p7.
81 The N-terminus and transmembrane domains were non-exchangeable and therefore constitute a
82 cross-species barrier in hepaciviral assembly. In contrast, the basic loop and the C-terminus of
83 NPHV p7 were readily exchangeable allowing production of infectious *trans*-complemented viral
84 particles. In conclusion, comparison of NPHV and HCV p7 revealed structural and functional
85 homology of these proteins including liposome permeability and broadly acting determinants
86 were identified which modulate hepaciviral virion assembly and contribute to the host-species
87 barrier.

88 **Importance**

89 The recent discovery of new relatives of hepatitis C virus (HCV) enables for the first time the
90 study of cross-species determinants shaping hepaciviral pathogenesis. Nonprimate hepacivirus
91 (NPHV) was described to infect horses and represents so far the closest homolog of HCV. Both
92 viruses encode the same viral proteins; however NPHV protein functions remain poorly
93 understood. In this study, we aimed to dissect NPHV p7 on a structural and functional level. By
94 using various NMR structures of HCV p7 as templates, three-dimensional homology models for
95 NPHV p7 were generated highlighting conserved residues being important for ion-channel
96 function. A p7-based *trans*-complementation approach and the construction of NPHV/HCV p7
97 chimeric viruses showed that the N-terminus and transmembrane domains were non-
98 exchangeable. In contrast, the basic loop and the C-terminus of NPHV p7 were readily
99 exchangeable allowing production of infectious viral particles. These results identify species-
100 specific constraints as well as exchangeable contaminants in hepaciviral assembly.

101

102 **Introduction**

103 For more than two decades, hepatitis C virus (HCV) and GB virus B (GBV-B) were the sole
104 members of the genus *Hepacivirus* within the *Flaviviridae* family. Recently, multiple new
105 hepaciviruses have been identified in dogs (1), horses (2), bats (3, 4), rodents (3, 5), non-human
106 primates (6), rats (7) and cattle (8, 9). Among them, nonprimate hepacivirus (NPHV), initially
107 described to infect dogs and subsequently horses, is the closest homolog of HCV and thus
108 represents a unique model to study differences in hepacivirus pathogenesis of HCV and HCV-
109 related viruses (10, 11).

110 HCV is globally distributed and approximately 146 million people of the world's population are
111 persistently infected (12). Individuals infected with HCV are at high risk of developing liver
112 cirrhosis and hepatocellular carcinoma (13). The development of direct-acting antivirals (DAA's)
113 has significantly improved antiviral treatment options (14). However, a prophylactic vaccine is
114 still lacking. The genome of HCV consists of a single-stranded RNA with positive polarity and
115 encodes for ten viral proteins in an open reading frame (ORF) (15). The small membrane protein
116 p7 is encoded between the structural proteins core, E1 and E2 and the non-structural proteins. P7
117 is classified into the group of viroporins since it fulfills major characteristics of this family for
118 instance its small size of 63 amino acids and its ability to form oligomeric, hydrophobic ion-
119 channels in the endoplasmic reticulum (ER) membrane (16). P7 is composed of two
120 transmembrane passages connected by a short polar loop. The N-terminal helix and C-terminus
121 are facing towards the lumen of the ER (17), however another topology where the C-terminus is
122 exposed towards the cytosol has also been reported (18). P7 monomers assemble to form
123 hexameric or heptameric structures (19-22). By applying single-particle electron microscopy a
124 three-dimensional model of a p7 hexamer was resolved (20). Additionally, the monomeric and
125 oligomeric structure of p7 of different genotypes was elucidated by nuclear magnetic resonance

126 spectroscopy (NMR) studies in different lipid-mimicking environments (TFE, DHPC, DPC or
127 methanol) (23-26), which likely explains the structural discrepancies observed between these
128 models. *In vitro* analysis revealed that p7 is essential for HCV assembly and release, whereas it is
129 dispensable for viral replication (27, 28). For further details on structural and functional
130 properties of HCV p7 see also recent reviews (16, 29, 30).

131 After the identification of NPHV, several studies have been conducted to investigate differences
132 and similarities between NPHV and HCV. A high seroprevalence of anti-NPHV antibodies (30-
133 40%) among horses was reported with 2-7% of the horses also carrying viral RNA (10). Similar
134 to HCV, also NPHV is a hepatotropic virus as was evidenced by accumulation of viral plus and
135 minus strand RNA in liver sections (31). The genomic organization of HCV and NPHV is highly
136 conserved with one ORF encoding the viral proteins (10, 11). As seen for HCV, the ORF of
137 NPHV is flanked by two untranslated regions (UTR) at the 5' and 3' end with the 5'UTR
138 displaying a larger stem loop I (2). Regarding the function of NPHV viral proteins, individual
139 expression of the NPHV core protein showed that core localizes on lipid droplets as reported for
140 HCV core (32). In addition, the NS3/4A protein of NPHV has been shown to have a similar
141 function as the HCV equivalent by cleaving human mitochondrial antiviral signaling protein
142 (MAVS) and Toll-IL-1 receptor domain-containing adaptor inducing interferon-beta (TRIF) (33).
143 However, a detailed understanding of viral protein function especially in the context of cross-
144 species determinants shaping hepaciviral pathogenesis is lacking.

145 In this study, we discovered that although NPHV p7 shared comparable structural features with
146 its human homolog and exerted an ion-channel activity, the protein could not fully substitute
147 HCV p7 during virus assembly. Replacement of the basic loop and the C-terminus within NPHV
148 p7, however, led to production of infectious HCV particles, thus defining virus species-specific
149 and interchangeable subdomains within p7.

150 **Materials and Methods**

151 **Sequence and phylogenetic analysis.** Nucleotide sequences of NPHV p7 isolates (GenBank
152 Accession numbers: KP325401, JQ434002, JQ434003, JQ434004, JQ434005, JQ434006,
153 JQ434007, JQ434008, JX948116; generated p7 sequences of this study are available upon
154 request) were translated and aligned using MEGA6 (34) and a consensus sequence was
155 generated. For phylogenetic analysis one representative p7 sequence of each HCV genotype was
156 utilized (GenBank Accession numbers: NC004102, YP001469630, NC009824, NC009825,
157 NC009826, NC009827, EF108306). The HCV p7 consensus sequence was deduced from the
158 ClustalW multiple alignment (35) of p7 sequences from representative HCV strains of confirmed
159 genotypes (as described in reference (23)). A Maximum Likelihood phylogenetic tree was
160 generated using MEGA6 (34).

161
162 **Structural analysis.** Three-dimensional homology models of NPHV p7 monomer were
163 constructed by the Swiss-Model automated protein structure homology modeling server
164 (<http://www.expasy.org/spdbv/>; (36)) by using the NMR structures of HCV p7 as templates (23-
165 26). Two models of the NPHV p7 three-dimensional hexamer were generated. The positions of
166 models 1 and 2 relatively to the membrane bilayer was deduced from molecular dynamics (MD)
167 simulations of HCV p7 in POPC bilayer as reported in Chandler *et al.* (19) and Kalita *et al.* (37),
168 respectively. Figures were generated from structure coordinates by using VMD
169 (<http://www.ks.uiuc.edu/Research/vmd/>; (38)) and rendered with POV-Ray
170 (<http://www.povray.org/>).

171
172 **Peptide synthesis of HCV and NPHV p7.** The p7 peptides of the JFH-1 or H14 strain were
173 synthesized with a CEM microwave peptide synthesizer. Therefore, all required amino acids were

174 dissolved in N,N-dimethylformamide (DMF; Rathburn Chemicals Ltd). As activator
175 hydroxybenzotriazole (HoBt) hydrate and as activator base N,N'-diisopropylcarbodiimide (DIC;
176 Sigma) were used. Deprotection was conducted in 20% piperidine (Sigma) in DMF (v/v).
177 Dichloromethane (Sigma) was used for washing. 16.4 l of DMF, 150 ml of activator, 200 ml of
178 activator base, 2.8 l of deprotect, 0.17 g of resin and 0.2 M of each respective amino acid were
179 placed in a CEM microwave peptide synthesizer and a programme was created to start synthesis
180 from the C-terminus. The first amino acid added was arginine (Arg), since alanine (Ala) is
181 attached to the resin. Reactions for all the amino acids were double coupling except proline.
182 Cycles for Arg, Cys and His are performed at lower temperature and for a longer time period to
183 avoid racemization. To avoid any side chain reaction only Fmoc-Lys (Boc)-OH for lysine (Lys)
184 was used with double coupling. The instrument will automatically stop and collect the resin with
185 synthesized peptide which is then required to cleave the peptide from resin. Peptides were
186 purified by HPLC on a C4-semipreparative column with a linear acetonitrile gradient. The purity
187 was verified by SDS PAGE. The sequence of the p7 peptide was confirmed by MALDI-TOF
188 mass spectromic analysis.

189
190 **Liposome permeability assay.** Liposome preparation and permeability assays were conducted as
191 described earlier (39). Briefly, lipids (Avanti Polar Lipids) in chloroform were added in a final
192 mixture containing 0.5 mg L- α -phosphatidic acid, 0.5 mg L- α -phosphatidyl choline and 0.5 %
193 w/w L- α -phosphatidyl ethanolamine with lissamine rhodamine B labelled head groups.
194 Chloroform was evaporated from the lipids using a stream of nitrogen, before placing in a
195 vacuum for 4 hours at room temperature (RT). Lipids were rehydrated to 2 mg/ml in a self-
196 quenching concentration of carboxyfluorescein (CF) buffer (50 mM 5(6)-Carboxyfluorescein
197 (SIGMA), 10 mM HEPES (pH 7.4), 107 mM NaCl) and vigorously shaken overnight at RT.

198 Unilamellar liposomes were produced using an extruder (Avanti Polar Lipids) and a 0.4 μm filter
199 (whatman). Liposomes were purified via centrifugation at 49 000 rpm for 15 min at 25°C
200 including 4 washing steps before the pellet was resuspended in 0.5 ml liposome assay buffer (10
201 mM HEPES, pH 7.4, 107 mM NaCl). For p7 activity assays the peptides were reconstituted in
202 100% DMSO and the concentration was determined by nanodrop. Liposomes supplemented with
203 1% v/v DMSO were used as a baseline for fluorescence. Assays were carried out in black-walled,
204 flat-bottomed black-base 96-well plates at 37°C. Each well contained 50 μM of liposomes
205 (calculated from the rhodamine fluorescence) and 1 μl of peptide in DMSO in a total volume of
206 100 μl with liposome assay buffer. 0.5 % v/v Triton TX-100, which lyses liposomes, was used
207 for gain adjustment, setting a level of 90% fluorescence. The 96-well plate was kept on ice for 2-
208 5 minutes after gain adjustment and while the peptide +/- drug was added. CF release measured
209 by increased fluorescence was taken as an indicator of peptide induced membrane permeability
210 (activity). A set of 30 readings (λ ex485/ λ em520 nm) was made over the course of 24 minutes
211 using a FLUOstar Galaxy plate-reader (BMG Labtech). Each condition was carried out in
212 duplicate wells with three independent experimental repeats. End point measurements were used
213 for the analysis with the average of the duplicate wells taken. For NN-DNJ inhibition assays
214 liposomes contained 2% v/v DMSO +/- 40 μM NN-DNJ, these being the respective background
215 levels for drug-free and drug-treated wells. As peptide concentrations 9 μM of NPHV p7 peptide
216 and 44 μM of JFH-1 p7 peptide were used. Peptides +/- inhibitor were incubated for 20 minutes
217 at RT prior to addition to the gain adjusted plate on ice. Statistical analysis was conducted by a
218 Welch's corrected unpaired t-test. P-values <0.05 were considered as statistical significant (*).

219
220 **Cell culture.** Huh-7.5 cells were cultured in Dulbecco's modified Eagle's medium (Life
221 Technologies) supplemented with 10 % fetal bovine serum (FCS), 2 mM L-glutamine,

222 nonessential amino acids (Invitrogen), 100 µg/ml streptomycin (Invitrogen) and 100 IU/ml
223 penicillin (Invitrogen) (DMEM complete) at 37°C and 5% CO₂. The packaging cell line Huh-
224 7.5[C][E1E2][NS2]J6 expressing the Jc1 derived proteins C, E1E2 and NS2 was generated by
225 lentiviral gene transfer as described earlier (40). Vectors used for the gene transfer encoded for a
226 blasticidin-S deaminase resistance gene and therefore 5 µg/ml of blasticidin (Invivogen) was
227 added for selection.

228

229 **Plasmids.** The plasmids and pFK-PI-Spp7/J6-EI-NS3-5B/JFH-1, pFK-PI-Sp-HA-HA-L-p7/J6EI-
230 NS3-5B/JFH-1 and pFK-PI-G-Luc-EI-NS3-5B/JFH-1 have been described earlier (41, 42) and
231 are based on the bicistronic helper replicon pFK-PI-EI-NS3-5B/JFH-1. This helper replicon
232 contains a poliovirus derived internal ribosomal entry site (IRES) (PI) downstream of the JFH-1
233 derived 5'-nontranslated region (5'NTR) (nucleotides 1 to 341 of JFH-1) and is separated by a
234 spacer region of 72 nucleotides. The second cistron is under the control of an
235 encephalomyocarditis virus IRES (EI) that expresses JFH-1 derived NS3 to NS5B proteins. The
236 p7 sequence of the NPHV isolate H14 and different HCV/NPHV p7 chimeras were chemically
237 synthesized (Integrated DNA Technologies, IDT). The cloned fragments included a signal
238 peptide (sp) derived from the last 51 base pairs of the E2 protein (HCV isolate J6) downstream of
239 the p7 sequence or additionally a HAHA-tag linked to the p7 sequence with a linker and upstream
240 of the sp. The respective genes were cloned into the first cistron of pFK-PI-EI-NS3-5B/JFH-1 by
241 restriction digest and ligation. In addition to bicistronic helper replicons used for trans-
242 complementation assays, experiments with the HCV full length virus were also performed.
243 Therefore the plasmids pFK-Jc1 (43), pFK-Jc1-Δp7half (27) and pFK-Jc1-HA-HA-L-p7/J6 (42)
244 were utilized. The p7 sequence of the NPHV isolate H14 and the p7 sequences of HCV/NPHV
245 chimeras (p7J6-loop-H14, p7J6-C-ter-H14 and p7J6-loop-C-ter-H14) were cloned into pFK-Jc1

246 and pFK-Jc1-HA-HA-L-p7/J6 by polymerase chain reaction (PCR)-based insertion. All
247 constructs were confirmed by sequencing prior to use. Further details regarding the cloning
248 strategies and exact nucleotide sequences are available upon request.

249
250 ***In vitro* transcription and electroporation.** *In vitro* transcripts were created according to the
251 protocol described previously (40). DNA was purified by the Qiaquick PCR purification kit
252 (Qiagen) and RNA was purified by the NucleoSpin RNA Extraction Kit (Macherey Nagel)
253 according to the manufacturer's instructions. Concentration was determined by nanodrop. *In vitro*
254 transcribed RNA was stored at -80°C until electroporation.

255 Electroporations were conducted as described earlier (40). Briefly, Huh-7.5 or Huh-
256 7.5[C][E1E2][NS2]J6 cells were trypsinized, taken up in DMEM complete and the cell number
257 was determined. A final concentration of 1.5×10^7 cells/ml in 400 μ l of Cytomix (120 mM KCl,
258 0.15 mM CaCl₂, 10 mM K₂HPO₄/KH₂PO₄ (pH 7.6), 25 mM HEPES, 2 mM EGTA, 5 mM
259 MgCl₂, adjust pH to 7.6 with KOH) supplemented with 2 mM ATP and 5 mM Glutathione per
260 electroporation and 5-10 μ g of *in vitro* transcripts were used per electroporation. Transfected
261 cells were directly taken up in 12-16 ml DMEM complete and seeded into 6-well plates or 10 cm
262 dishes depending on the application.

263
264 **Immunofluorescence.** After transfection, cells were seeded into a 24-well plate onto coverslips.
265 Cells were fixed 48 h post transfection by addition of 3% paraformaldehyde. Staining of
266 intracellular HAHA-tagged p7 and a co-staining of E2 or NS3 was performed as described
267 elsewhere (42). In brief, fixed cells were permeabilized with 0.5% Triton-X100 for 10 minutes at
268 RT. Blocking was conducted for one hour at RT in blocking buffer (5% goat serum (Sigma) in
269 PBS). The primary antibodies were incubated overnight at room temperature in blocking buffer.

270 The primary mouse α -HA antibody (Covance) was diluted 1:1000, the primary rabbit α -NS3
271 4949 (44) was diluted 1:400 and the primary human α -E2 antibody CBH-23 (45) was diluted
272 1:250 in blocking buffer. The α -NS3 and α -E2 antibodies were kind gifts from R. Bartenschlager
273 (University of Heidelberg) and S. Fong (Stanford University), respectively. Species-specific
274 secondary antibodies (A488-conjugated α -mouse IgG, A546-conjugated α -rabbit IgG and A546-
275 conjugated α -human IgG) were diluted 1:1000 in blocking buffer and incubated for 1 hour at RT
276 in the dark. Cell nuclei were stained with DAPI (Invitrogen). Last, coverslips were mounted on
277 glass slides using Fluoromount-G (Southern Biotech). Pictures were taken using a x100
278 magnification lens by an inverted confocal laser-scanning microscope (Olympus Fluoview 1000).
279 A sequential acquisition mode with an average of 3 frames for each picture (Kalman n=3) was
280 applied for the 3 channels used.

281

282 **Western blot.** Western blot analysis of cell lysates was performed as previously described (42).
283 Briefly, cells were lysed 48 h post transfection by addition of 1% Triton-X100 supplemented
284 with protease inhibitor (Roche). Nuclei were separated by centrifugation and reducing sample
285 buffer was added to the supernatant. Samples were incubated at 37°C for 15 minutes prior
286 separation by SDS-PAGE. After transfer of the separated proteins on a membrane, the membrane
287 was incubated for 1 h in blocking solution (5% milk in 0.05% Tween/PBS). The primary
288 antibody was incubated over night at 4°C in blocking solution. The following dilutions were used
289 for the antibodies: mouse α -HA (Sigma) 1:1000; mouse α -NS5A 9E10 (46) 1:1000; mouse α -
290 NS2 6H6 (47) 1:1000; mouse α -E2 AP33 1:1000; mouse α - β actin (Sigma) 1:1000. The α -NS5A
291 9E10 and α -NS2 6H6 antibodies were a generous gift from C. M. Rice (Rockefeller University).
292 The α -E2 AP33 antibody was provided by Genentech and Arvind Partel (University of Glasgow)
293 (48). The secondary horseradish peroxidase-conjugated (HRP)-coupled antibody (α -mouse,

294 Sigma) was incubated for 1 h at room temperature. It was diluted 1:20 000 except after
295 incubation with the α -HA antibody (1:2000). After washing in 0.05% Tween/PBS,
296 chemiluminescence was obtained with the ECL Plus Western Blotting Detection System (GE
297 Healthcare) and measured using a ChemoCam Imager.

298

299 **Virus titration.** To determine viral titers in collected supernatants, a limiting dilution assay was
300 conducted on Huh-7.5 cells. The 50% tissue culture infectious dose (TCID₅₀) was determined 72
301 h post infection as reported earlier (40).

302

303 **Results**

304 **NPHV p7 amino acid sequence is highly conserved and shows structural features**
305 **comparable to HCV p7**

306 To examine the degree of p7 amino acid sequence conservation among different NPHV p7
307 isolates, 15 distinct NPHV p7 sequences were aligned and a consensus sequence was generated
308 (Fig. 1A). The identification of the respective NPHV p7 sequences was based on cleavage site
309 predictions as reported earlier (11). Overall, the NPHV p7 sequences were highly conserved at
310 the amino acid level with only 11 positions (over the 63 residues) showing some variations (Fig.
311 1A). Alignment of globally sampled NPHV and HCV p7 nucleotide sequences and subsequent
312 phylogenetic analysis revealed a high level of divergence between HCV and NPHV, with each
313 virus forming a discrete, well supported clade (Fig. 1B). Of note, sampled NPHV p7 isolates
314 showed a remarkably lower nucleotide variation when compared to HCV p7 isolates derived
315 from genotypes (GT) 1-7, which is indicated by the different branch lengths (Fig. 1B). Database
316 searching for proteins related to NPHV p7 using either Blast (49) or Fasta (50) revealed that p7
317 from HCV genotype 4f displays the highest similarity to the NPHV consensus sequence, with
318 33% of identical amino acids and 28% and 13% of strongly and weakly similar amino acids.
319 Moreover, similar percentages were observed when comparing the NPHV p7 consensus sequence
320 with p7 consensus sequences from representative HCV strains of confirmed genotypes (51, 52)
321 (19% identical, 24% strongly similar, 16% weakly similar and 30% different residues; Fig. 2A).
322 With respect to the non-conserved residues, one can distinguish those exhibiting obvious
323 physicochemical differences (colored dark blue in Fig. 2A) from those for which the hydrophobic
324 or hydrophilic character is conserved (colored light blue). Moreover, most of the latter NPHV p7
325 residues could be observed as minor variants in the p7 amino acid repertoire of HCV reference
326 genotypes (reported in Fig. 2A in (27); residue positions 11, 22, 37, 44, 45 and 51). In total, only

327 20% of residue positions distributed along the sequence appeared to be clearly specific for NPHV
328 and HCV p7, including positions 1, 5, 7, 9, 13, 14, 16, 29, 33, 39, 43, 46 and 47. Altogether,
329 these data indicate that the overall structure of NPHV p7 should be comparable to that of HCV
330 p7. This was also supported by secondary structure analyses and predictions of transmembrane
331 segments, which exhibited similar patterns for NPHV and HCV p7 (data not shown).

332 Several NMR structures have been reported for HCV p7 (19, 23-26) allowing us to construct
333 three-dimensional homology structure models for NPHV p7 by using the Swiss-Model automated
334 protein structure homology modeling server (<http://www.expasy.org/spdbv/>; (36)) and the
335 consensus NPHV p7 sequence as input. The four resulting homology structure models for the
336 monomeric form of NPHV p7 are depicted in Figure 2B. The three first models exhibited a
337 “hairpin-like” topology consisting of two transmembrane segments that are connected by a
338 hydrophilic, positively charged cytosolic loop containing residues 33 and 35. According to the
339 corresponding hexameric forms of these models (19, 24, 25) and to the typical oligomeric
340 structure of viroporins (53), NPHV p7 subunits would reside side-by-side as illustrated by model
341 1 in Figure 2C. In contrast, NPHV p7 homology model based on the NMR structure of hexameric
342 p7 reported by Ouyang *et al.* (26) would exhibit an unusual architecture where part of each p7
343 subunit crosses over to interact with other p7 subunits that are not its neighbors (model 2, Fig.
344 2C). Nevertheless, these models allowed the positioning of conserved, very similar, similar,
345 different and very different residues (colored from red to blue, respectively) along the secondary
346 structure elements for each model (Fig. 2B) as well as at the surface of hexamer models and
347 within their ion-channel pores (Fig. 2C).

348

349 **NPHV p7 exerts an ion-channel activity in a liposome permeability assay**

350 As the NPHV p7 structural analyses revealed similar features to HCV p7, we next used the
351 liposome permeability assay previously reported for HCV p7 (39) to evaluate its ion-channel
352 features. To produce the respective p7 peptides of NPHV (isolate H14) and HCV (isolate JFH-1),
353 a chemical synthesis was performed (see Material and Methods). The p7 peptides were
354 reconstituted in DMSO and validated using mass spectrometry and SDS-PAGE, before
355 increasing doses of the peptides were incubated with liposomes previously loaded with
356 carboxyfluorescein (CF) at self-quenching concentrations. In this assay, increase in membrane
357 permeability was measured by the dye release and dequenching. An increase of fluorescence was
358 observed when the NPHV p7 peptide was added to the liposomes, which reached a plateau with a
359 peptide concentration of 10-20 μ M (Fig. 3A). The HCV JFH-1-derived peptide demonstrated an
360 ion-channel activity in a dose-dependent manner with about 2-3-fold higher fluorescent units
361 (FU) compared to NPHV p7 (Fig. 3B). As the iminosugar derivative *N*-nonyl-deoxynojirimycin
362 (*NN*-DNJ) was reported to block the HCV p7 ion-channel activity (54), we analyzed the
363 inhibitory effect of *NN*-DNJ against NPHV p7. As depicted in Figure 3C, NPHV p7-dependent
364 permeabilization of liposomes could be blocked with 40 μ M *NN*-DNJ in a similar fashion as
365 HCV p7 (Fig. 3C). Taken together, similar to HCV p7, these data indicate that NPHV p7 is likely
366 able to exert an ion-channel function which can be blocked by iminosugar derivatives.

367
368 **Cross-species substitutions of the basic loop and the C-terminus in p7 lead to production of**
369 ***trans*-complemented particles**

370 To study the capability of NPHV p7 to rescue production of infectious particles, we made use of
371 a p7-based HCV *trans*-complementation system (41). This system permits the evaluation of p7
372 function in virus-producing cells independently of secondary effects on polyprotein processing.
373 The p7 sequence originating from the NPHV isolate H14 was cloned into the first cistron of a

374 bicistronic JFH-1 helper replicon (Fig. 4A). The p7 sequence was located downstream of a signal
375 peptide (sp) sequence encompassed within the last 51 amino acids of the HCV E2 protein derived
376 from the J6 isolate. Additionally and to facilitate p7 detection, another construct containing a sp,
377 HAHA-tag and a short linker sequence (GGGGSG) connected to NPHV p7 H14 was created. The
378 analogous constructs containing HCV p7 of the isolate J6 or the *Gaussia*-Luciferase gene (G-
379 Luc), both previously described (41, 42), were utilized as positive and negative controls,
380 respectively. The second cistron encoded for the non-structural proteins NS3-NS5B from the
381 HCV isolate JFH-1. *In vitro* transcripts of these constructs were individually transfected into a
382 packaging cell line encoding for the remaining viral proteins, core (C), E1E2 and NS2 from the
383 HCV isolates J6 and JFH-1 (Fig. 4A). To confirm the expression of HAHA-tagged p7, we
384 performed Western blot analysis showing that both HAHA-tagged p7 J6 and HAHA-tagged p7
385 H14 were expressed (Fig. 4B). However, in the lysate of HAHA-tagged p7 H14 additional
386 proteins with a higher molecular weight were detected (Fig. 4B) indicating SDS-resistant
387 oligomeric forms of the HAHA-tagged p7. Next, we analyzed the sub-cellular localization of
388 HAHA-tagged p7 in fixed cells by indirect fluorescence microscopy using antibodies recognizing
389 the HA-tag, HCV NS3 or E2 proteins in order to permit the assessment of co-localization
390 between these polypeptides (Fig. 4C). Both HAHA-tagged p7 proteins, J6 and H14, showed a
391 similar localization in the cytoplasm at ER membranes by co-localizing with E2 and NS3. The
392 rescue of HCV particle production by NPHV p7 was assessed after transfection of the packaging
393 cell line with the different p7 variants and infectivity released into the cell culture supernatant of
394 transfected cells. The J6-derived p7 construct could be rescued with peak titers of 5×10^4
395 TCID₅₀/ml, while the double HA-tagged genome produced lower viral progeny as previously
396 reported (42). In contrast, NPHV p7 (with or without epitope tag) could not substitute the HCV

397 p7 function in this *trans*-complementation setting suggesting genetic incompatibilities between
398 NPHV p7 and HCV proteins.

399 To explore if NPHV p7 and HCV p7 contain virus-specific but potentially also interchangeable
400 (thus functionally conserved) subdomains, we replaced parts of HCV p7 with sequences of
401 NPHV p7. To this end, we constructed eleven distinct chimeras by dividing p7 into the N-
402 terminal, transmembrane helix 1 (TM1), basic loop, transmembrane helix 2 (TM2) and C-
403 terminal subdomain (Fig. 5A). All chimeric constructs were N-terminally tagged with a double
404 HA-tag connected by a short linker and preceded by a signal peptide sequence. These sequences
405 were cloned into the first cistron of a bicistronic JFH-1 helper replicon and *in vitro* transcripts
406 were transfected into Huh-7.5[C][E1E2][NS2]J6 packaging cells analogous to Figure 4A.
407 Expression of HAHA-tagged p7 variants was assessed by immunofluorescence analysis showing
408 the expression of chimeras 1, 2, 3, 5 and 11 and low or undetectable expression for the remaining
409 constructs (Fig. 5B) indicating an early degradation or a general incompatibility between HCV p7
410 and NPHV p7 parts. Next, we investigated the capability of these p7 chimeras to *trans*-
411 complement the production of infectious particles. The p7 chimeras 3 (replacement of the loop,
412 subsequently termed p7J6-loop-H14), 5 (replacement of the C-terminus, subsequently termed
413 p7J6-C-ter-H14) and 11 (replacement of the loop and C-terminus, subsequently termed p7J6-
414 loop-C-ter-H14) were able to produce infectious particles (Fig. 5C). Viral titers of about 1-2
415 orders of magnitude lower compared to p7J6 were observed with p7J6-C-ter-H14 showing the
416 highest titers. Replacement of the loop decreased the viral titers about 50-fold more drastically
417 and delayed the virus kinetics. To further examine the functionality of these chimeras, the
418 bicistronic replicons encoding for p7J6, p7H14, p7J6-loop-H14, p7J6-C-ter-H14 and p7J6-loop-
419 C-ter-H14 N-terminally linked to a signal peptide were co-transfected into Huh-7.5 cells with
420 Jc1Δp7_{half}, a HCV full length mutant described to completely abrogate viral particle production

421 (27) (Fig. 5D). As shown in Figure 5E, p7J6 as well as p7J6-loop-H14, p7J6-C-ter-H14 and p7J6-
422 loop-C-ter-H14 were able to rescue infectious particle production (Fig. 5E). In conclusion, cross-
423 species determinants in the basic loop and the C-terminus of hepaciviral p7 could be identified by
424 using a p7-based *trans*-complementation system.

425

426 **Cross-species determinants of NPHV p7 are important in late steps of the viral life cycle**

427 After the identification of cross-species determinants in hepaciviral virion production by creating
428 HCV/NPHV p7 chimeras, we next validated their functionality in the context of full-length HCV
429 cell culture derived particles (HCVcc). Hence, we cloned p7J6-loop-H14, p7J6-C-ter-H14, p7J6-
430 loop-C-ter-H14 and p7H14 into Jc1 and Jc1 HAHA-L-p7 (Fig. 6A). As positive control we
431 included the HCV constructs Jc1 and Jc1 HAHA-L-p7J6. These genomes were transfected into
432 Huh-7.5 cells and expression of epitope-tagged p7 was visualized 48 h later by Western blot
433 analysis. For the positive control Jc1 HAHA-L-p7J6 HAHA-tagged p7 could be detected as well
434 as the precursor proteins p7-NS2 and E2-p7-NS2 (Fig. 6B). In case of HAHA-L-p7H14 cleavage
435 defects were noted with signals at a molecular weight of approximately 24 kDa and 50 kDa
436 suggesting processing defects due to the insertion of H14 p7 into Jc1 (Fig. 4B). These proteins
437 were also detected for p7J6-loop-H14 and p7J6-loop-C-ter-H14, but here also free p7 was visible.
438 The p7J6-C-ter-H14 chimera showed an HA-detection pattern like the parental construct (Fig.
439 6B) indicating processing defects possibly at the E2/p7 junction or different oligomerization
440 forms. In addition, Western blot analysis to visualize NS2 and E2 in the same cell lysates was
441 conducted showing that only the precursor p7NS2 and no free NS2 can be detected for Jc1
442 HAHA-L-p7H14 (Fig. 6C).

443 Next, the release of infectious viral particles for the Jc1 constructs (Fig. 6D) and Jc1 HAHA-L-p7
444 (data not shown) constructs was determined by TCID₅₀ at different time points post transfection.

445 All HCV/NPHV epitope-tagged p7 chimeras led to the production of infectious particles while
446 displaying delayed time kinetics and lower titers compared to Jc1 HAHA-L-p7J6 (data not
447 shown). Moreover, as reported previously (42), these titers were around one order of magnitude
448 lower compared to the untagged constructs shown in Figure 6D. Jc1 p7J6-loop-C-ter-H14
449 showed the lowest production of infectious particles, whereas Jc1 p7H14 was not able to produce
450 infectious particles, which is in concordance to the results in the *trans*-complementation system.
451 As HCV p7 was reported to be important for the assembly and release step of the viral life cycle
452 (27, 28, 41), we investigated whether this function was also conserved in the context of the p7
453 chimeric genomes. To this end, we determined extra- and intracellular core amounts 48 h post
454 transfection (Fig. 6E) and calculated the specific infectivity for each construct (Fig. 6F). The
455 intracellular core amounts were comparable for all constructs, whereas the recombinant chimeric
456 constructs displayed a reduction in extracellular levels of core with Jc1 p7H14 at background
457 levels in line with the results from the infection assay (Fig. 6E). Therefore, the specific infectivity
458 of Jc1 p7J6-loop-H14 and Jc1 p7J6-C-ter-H14 was comparable to Jc1 demonstrating an
459 importance of NPHV p7 in viral assembly and release of infectious particles rather than in virus
460 entry. In case of the Jc1 p7J6-loop-C-ter-H14 the infectivity levels and extracellular core amounts
461 were minimal, therefore no specific infectivity could be calculated. Taken together, HCV/NPHV
462 p7 chimeras defining cross-species determinants of virion assembly were functional in the
463 context of HCV cell culture particles and were crucial for the late steps of the viral life cycle.

464
465 **Virion production of HCV/NPHV p7 chimeras can be inhibited by prototypic ion-channel**
466 **blockers**

467 Inhibitors including rimantadine and iminosugar derivatives blocking the ion-channel function or
468 oligomerization of HCV p7 have been described (55), but their detailed mechanism of action is

469 not well defined. To facilitate the understanding of p7 inhibitor functions and evaluate the ion-
470 channel activity of the HCV/NPHV p7 chimeras in the context of the complete viral life cycle,
471 we next tested the antiviral activity of the prototypic ion-channel inhibitors rimantadine (Fig. 7A)
472 and two iminosugars *N*-nonyl-deoxygalactonojirimycin (*NN-DGJ*) (Fig. 7B) and *N*-nonyl-
473 deoxynojirimycin (*MN-DNJ*) (Fig. 7C) against Jc1 p7J6-loop-H14 and Jc1 p7J6-C-ter-H14.
474 Inhibitors were added to cells 4 h post transfection and viral titers were determined 48 h post
475 transfection. Jc1 p7J6-loop-H14 was inhibited by rimantadine, *NN-DGJ* and *MN-DNJ* to a similar
476 level as the Jc1 wildtype (Fig. 7A, B and C). In contrast, Jc1 p7J6-C-ter-H14 showed a slightly
477 higher resistance profile to rimantadine and *NN-DGJ* compared to the parental Jc1 construct (Fig.
478 7A and B) indicating a lower binding affinity and less inhibitory activity of these inhibitors when
479 structural changes occur at the C-terminus of p7. These results indicate that in the context of
480 HCV/NPHV p7 chimeric viruses functional ion-channels are formed which can be inhibited by
481 specific p7 inhibitors.

482

483 **Discussion**

484 In this study, we performed a comparison of NPHV and HCV p7 on a structural and functional
485 level. Sequence alignment of reported and novel p7 isolates revealed a high level of conservation
486 among all isolates, especially when compared to the variation apparent among HCV isolates. This
487 is in accordance with the overall high conservation of the full NPHV genome between different
488 isolates, where a diversity of approximately 15% was reported in contrast to 30% of diversity
489 between HCV isolates (10). Amino acid sequence similarities indicate that the overall structure of
490 NPHV p7 is comparable to that of HCV p7, allowing us to construct NPHV p7 homology models
491 using reported three-dimensional NMR-based HCV p7 structures (19, 23-26) as templates for
492 monomeric and hexameric models. A greater degree of amino acid identity was found in the C-
493 terminal 48-63 p7 segment, including conservation of the upstream cleavage site of the signal
494 peptidase at the p7-NS2 junction. Despite the amino acid variability in 37-47 segment when
495 compared to HCV p7, the overall C-terminal half of p7 NPHV exhibits the characteristic
496 structural features of a signal peptide (Fig. 2A), and thus likely acts as a signal for the re-
497 initialization of translocation of the C-terminal part of p7. Interestingly, most of the different
498 residues in this segment are located at the surface of the hexamer homology models, and thus
499 should not disturb ion-channeling function of p7, but could potentially play a role in p7
500 interactions with other viral or cellular partners. Additionally, a high degree of amino acid
501 similarity was found in segment 17-32, which is thought to be the main structural element
502 involved in p7 pore formation and function. An interesting difference is the presence of only one
503 basic residue at position 35 in the putative cytosolic loop of NPHV p7 instead of two fully
504 conserved basic residues at positions 33 and 35 in p7 of all HCV genotypes (17). This suggests
505 that the basic residue at position 33 in HCV might be not essential for p7 functioning. Moreover,
506 the N-terminal segment 1-16 exhibited lower similarity with several different residues located

507 both at the surface of the hexamer models or facing the pore lumen. These features suggest that
508 this relatively poorly homologous segment should not play a critical role in ion-channeling but
509 could be important for specific interactions with other viral and/or host-specific cellular factors.
510 Moreover, as observed in HCV p7, this N-terminal segment also might play an essential role in
511 the complex mechanism of E2-p7 processing by signal peptidase (56, 57). Together, all these
512 structural features indicate a possible ion-channel function of NPHV p7 similar to HCV p7,
513 which is supported by the results of the liposome permeability assay. For chemically synthesized
514 p7 peptides of NPHV and HCV an increase of CF release with a concurrent increase of the
515 peptide concentration was observed. However, due to the property of the NPHV p7 peptide to
516 form aggregates at high concentrations, the effect was observed at lower peptide concentrations
517 and at an early peak compared to the HCV p7 peptide. The observed CF release could be blocked
518 by addition of the iminosugar NN-DNJ indicating an ion-channel function of NPHV p7. The
519 dibasic motif K33-R35 of HCV p7 was reported earlier to be important to maintain the ion-
520 channel activity in liposomes (58). Importantly and in line with the structural analysis of NPHV
521 p7, only the basic residue at position 35 is conserved in NPHV p7 and not the basic residue at
522 position 33, leading to the assumption that specifically residue 35 is essential to preserve p7
523 function.

524 We next investigated NPHV p7 determinants specific to NPHV or conserved between HCV and
525 NPHV. Moreover, we analyzed its sub-cellular localization and its role in the viral life cycle. By
526 using a p7-based *trans*-complementation approach, which is independent of viral polyprotein
527 processing, we could show that NPHV p7 was successfully expressed despite the detection of
528 oligomeric forms of NPHV p7. These oligomeric intermediates have not been observed for HCV
529 p7 so far. Nevertheless, the successful expression of NPHV p7 allowed us to investigate the sub-
530 cellular localization in infected cells. The highest degree of co-localization of HCV p7 with viral

531 proteins has been described for E2, whereas also co-localization with NS2, NS3, NS5A and in
532 parts core were reported (42). This is in accordance with our localization analysis showing that
533 epitope tagged NPHV p7 co-localizes with NS3 and E2 in a similar pattern as epitope tagged
534 HCV p7 in the cytoplasm of the cell. Despite the expression of NPHV p7 and sub-cellular
535 localization similar to HCV p7, no infectious particles were produced in the *trans*-
536 complementation system probably due to genetic incompatibilities of viral proteins. We could
537 demonstrate previously that even the replacement of genotype 2a J6-p7 by another HCV isolate
538 Con1 (genotype 1b) fully abrogated HCV particle production and even replacement by p7 of
539 another genotype 2a isolate (JFH-1) did significantly reduce the release of infectious particles
540 (27, 41). To overcome these cross-species genetic incompatibilities, HCV/NPHV p7 chimeras
541 were constructed demonstrating that the basic cytosolic loop and C-terminus of NPHV p7 as well
542 as the combination of both are interchangeable between NPHV and HCV thus restoring HCV
543 infectious particle production. For HCV, inter-genotypic p7 chimeras were also analyzed for
544 being infectious *in vivo* when the N-terminal and C-terminal tails of p7 from a genotype 1a virus
545 were maintained, but other parts substituted by genotype 2a sequences (59). Moreover, we
546 observed that the basic loop could be substituted without abolishing particle formation underlying
547 the importance of the basic residue 35 to maintain NPHV p7 functions. Lastly, we tested the
548 generated chimeras as well as the full NPHV p7 sequence in an HCV full-length virus (HCVcc)
549 revealing comparable virion production to the *trans*-complementation system that the complete
550 NPHV p7 sequence could not compensate for HCV p7 function due to cross-species
551 incompatibilities. In addition, Western blot analysis showed an absence of mature NPHV p7 with
552 the correct molecular weight. However, the detected proteins coincide with the molecular weight
553 of the proteins detected in the *trans*-complementation system, where no precursor proteins are
554 produced indicating an oligomerization of NPHV p7 rather than a cleavage defect. Nevertheless,

555 the novel chimeras were fully functional and were shown to be important for viral assembly and
556 release. Thus, virus-specific determinants of hepaciviral virion assembly are located in the N-
557 terminus and transmembrane regions of p7.

558 Inhibitor experiments with rimantadine and the iminosugar derivatives *NN-DGJ* and *NN-DNJ*
559 were conducted since these prototypic ion-channel inhibitors were reported to target HCV p7 and
560 reduce particle production (60). These experiments showed that the HCV/NPHV p7 chimera
561 carrying the C-terminus of NPHV p7 was more resistant especially to rimantadine and *NN-DGJ*
562 at high concentrations. The interaction sites of rimantadine with HCV p7 were analyzed
563 previously (24) showing key interacting residues at position 46, 48 and 52, which are present in
564 the chimeric construct. However, the change of the C-terminus of p7 could influence the overall
565 p7 folding, which could compress the rimantadine binding cavity leading to a less favourable fit
566 for the molecule resulting in a more drug-resistant phenotype. The iminosugar derivative *NN-*
567 *DNJ* demonstrated an inhibition of all viruses at the highest concentration, which may results not
568 only from the p7 ion-channel inhibition, but also from the blockage of ER α -glucosidases
569 required for folding and maturation of the HCV glycoproteins (60).

570 In conclusion, the identification of viruses closely related to HCV allowed for the first time a
571 cross-species comparison of two naturally occurring hepaciviral species. We could show that the
572 overall structure of NPHV p7 is highly conserved compared to HCV p7 and that NPHV p7 most
573 likely exhibits an ion-channel activity. Molecular analysis revealed a similar sub-cellular
574 localization of NPHV p7 with an ER-like pattern. Moreover, although NPHV p7 could not fully
575 replace HCV p7 function, the basic loop and C-terminus could be substituted leading to the
576 production of infectious particles. The results implicate a similar role of NPHV p7 in viral
577 pathogenesis as seen for its human homolog and identify broad hepaciviral protein determinants
578 for virus assembly.

579
580

581 **Figure legends**

582 **Figure 1**

583 **Sequence and phylogenetic analysis of NPHV p7.** A) Amino acid conservation in NPHV p7.

584 Top panel represents a sequence logo (61) of the 63 amino acid NPHV p7 ion-channel generated

585 from an alignment of 15 globally sampled strains (GenBank Accession numbers: KP325401,

586 JQ434002, JQ434003, JQ434004, JQ434005, JQ434006, JQ434007, JQ434008, JX948116;

587 generated p7 sequences of this study are available upon request). Nucleotide sequences were

588 translated and aligned using MEGA6 (34). Individual amino acids are color-coded according to

589 physiochemical properties and individual residue frequencies in the population are proportional

590 to the x-axis. The global NPHV p7 consensus sequence is positioned directly below with *

591 indicating complete conservation at the amino acid level in all sampled strains. B) Phylogenetic

592 comparison of NPHV and HCV p7. NPHV and HCV p7 nucleotide sequences (189 bp) were

593 aligned and a Maximum Likelihood phylogenetic tree generated using MEGA6 (34). NPHV p7

594 sequences represent all available reported sequences downloaded from GenBank, in addition to

595 sequences generated in this study (GenBank Accession numbers: KP325401, JQ434002,

596 JQ434003, JQ434004, JQ434005, JQ434006, JQ434007, JQ434008, JX948116, H10, H14-H18).

597 HCV p7 sequences represent a single isolate from genotypes (GT) 1-7 (GenBank Accession

598 numbers: NC004102, YP001469630, NC009824, NC009825, NC009826, NC009827,

599 EF108306). Branch lengths are proportional to the scale bar and equivalent to genetic distance

600 measured in nucleotide substitutions per site.

601

602 **Figure 2**

603 **Homology structure models of NPHV p7.** A) Comparison of the NPHV p7 consensus sequence

604 (see also Fig. 1) to HCV p7 consensus sequence. The degree of amino acid physicochemical

605 conservation at each position is inferred with the similarity index according to ClustalW
606 convention (asterisk, invariant, red; colon, highly similar, dark pink; dot, similar, pink). Non-
607 conserved but slightly different residues are colored light blue, while very different residues are
608 colored dark blue. Underlined residues correspond to positions exhibiting conserved aromatic
609 residues. Positions 33 and 35 in the central cytosolic loop are boxed. Note that the C-terminal
610 half part of p7 exhibits structural features that are characteristic of signal peptides (62), consisting
611 of an N-terminal region (n-domain) encompassing 1–3 positively charged residues (Arg), a
612 hydrophobic core region (h-domain) forming an alpha-helix, and a more polar, flexible region (c-
613 domain) containing a signal peptidase cleavage site; residues at positions -1 and -3 relative to the
614 cleavage site are small neutral residues (Ala) and form the recognition site for signal peptidases
615 (63), whereas alpha-helix-destabilizing residues (Pro, Gly) are present at position -6 and/or in the
616 middle of the h-domain. B) Ribbon representation of the three-dimensional homology models of
617 NPHV p7 monomer. Four previously published NMR-based structures were used as templates for
618 modeling (23-26). Left, p7 monomer structure determined by NMR in 50% TFE and molecular
619 dynamic (MD) simulations ((23); PDB entry); middle left, NMR-based structure of p7 monomer
620 determined in 125 mM DHPC ((25); PDB entry, 2MTS); middle right, Flag-p7 monomer
621 structure determined in 100% MeOH ((24); PDB entry, 3ZD0; the Flag tag and C-terminal
622 extension are not shown); right, one subunit of hexamer p7 NMR structure model determined in
623 200 mM DPC ((26); PDB entry, 2M6X). N- and C-termini are noted by “N” and “C”,
624 respectively. Alpha-helical segments are indicated and residues are color-coded according to
625 panel A. Residues 33 and 35 side-chain atoms are represented as van der Waals spheres and
626 illustrate the location of the central cytosolic loop of p7. C) Three-dimensional homology models
627 1 and 2 of NPHV p7 hexamer using the HCV p7 NMR/MD model in POPC of Chandler *et al.*
628 ((19); model 1) and the HCV p7 NMR model in DPC of Ouyang *et al.* ((26); model 2) as

629 templates. Two opposing subunits are shown in the left. Hexameric forms of NPHV p7 models
630 are in surface representations from different viewpoints: middle left, side view of the hexamer
631 surface; middle right, sectional view showing the pore interior with its axis symbolized by the
632 dashed line; right, ER lumen view showing the pore. Residues are color-coded according to panel
633 A and B. Thick green lines shown in the left hand panels represent the polar membrane bilayer
634 interfaces and hydrophobic core (between the middle two lines).

635

636 **Figure 3**

637 **Evaluation of the NPHV p7 ion-channel activity in a liposome permeability assay.** The HCV
638 and NPHV p7 peptides were chemically synthesized and used for subsequent liposome
639 permeability assays. P7 peptides originating from the A) NPHV isolate H14 and B) HCV isolate
640 JFH-1 were reconstituted in DMSO. Different concentrations of peptide were added to 50 μ M of
641 carboxyfluorescein loaded liposomes and the fluorescence units [FU] were measured as an
642 indicator of peptide-induced membrane permeability (activity). Liposomes supplemented with
643 1% v/v DMSO were used as solvent control. Three independent experiments in duplicate wells
644 were conducted and mean values +/- SD are depicted. C) Inhibition assays with NN-DNJ were
645 conducted. Therefore, liposomes contained 2% v/v DMSO +/- 40 μ M NN-DNJ, these being the
646 respective background levels for drug-free and drug-treated wells. As peptide concentrations 9
647 μ M of NPHV p7 peptide and 44 μ M of JFH-1 p7 peptide were used. Peptides +/- inhibitor were
648 incubated for 20 minutes at RT prior to addition to the gain adjusted plate on ice. Three
649 independent experiments in duplicate wells were conducted. Depicted is the mean value +SD
650 normalized to the respective solvent control. The percentage of inhibition was calculated by
651 normalizing to the DMSO control without inhibitor. Statistical analysis was conducted by a
652 Welch's corrected unpaired t-test. P-values <0.05 were considered as statistical significant (*).

653

654 **Figure 4**

655 **Analysis of NPHV p7 in a *trans*-complementation setup.** A) Experimental setup. The p7
656 sequence of the HCV isolate J6 and of the NPHV isolate H14 (sequence available upon request)
657 were cloned either untagged or linked to a HAHA-tag into the first cistron of a bicistronic helper
658 replicon as previously reported (42). The signal peptide-coding sequence (sp) corresponded to the
659 last 51 base pairs from the E2 J6 sequence was cloned downstream of p7. The insertion of a
660 *Gaussia* luciferase (G-Luc) served as a negative control. The second cistron encodes for the non-
661 structural proteins NS3-NS5B originating from the HCV isolate JFH-1. These bicistronic helper
662 replicons were individually transfected into a packaging cell line expressing the remaining viral
663 proteins core (C), E1E2 and NS2 from the HCV isolate J6. B) The expression of HAHA-tagged
664 p7 in cell lysates was confirmed 48 h post transfection by Western blot analysis. Additionally, the
665 viral protein NS5A and a cellular protein β -actin were stained. C) Co-staining of NS3 and
666 HAHA-tagged p7 (upper panel) and of E2 and HAHA-tagged p7 (lower panel) was performed 48
667 h post transfection on fixed cells. Depicted in gray are single stainings with DAPI, α -HA, α -NS3
668 and α -E2 as well as a colored merge pictures. Here, cell nuclei are shown in blue, α -HA staining
669 in green, and α -NS3 and α -E2 are shown in red, respectively. Pictures were taken using a 100x
670 magnification lens. D) Viral titers in supernatants 24 h, 48 h and 72 h post transfection were
671 determined by TCID₅₀. The mean of three independent experiments is depicted as log₁₀
672 TCID₅₀/ml + standard deviation (SD).

673

674 **Figure 5**

675 **Construction of HCV/NPHV p7 chimeras in a *trans*-complementation system.** A) Eleven
676 distinct HCV/NPHV p7 chimeras were constructed by dividing p7 into 5 parts (N-terminus,

677 transmembrane helix 1 (TM1), loop, transmembrane helix 2 (TM2) and C-terminus,
678 respectively). As templates the HCV isolate J6 and the NPHV isolate H14 were utilized and their
679 respective amino acid sequences are depicted. Amino acid sequences originating from H14 are
680 shown as light gray bars, whereas amino acids originating from J6 are shown as dark gray bars.
681 P7 chimeras were cloned into the bicistronic helper replicon including a signal peptide, a HAHA-
682 tag and a short linker according to Figure 4A. Constructed bicistronic helper replicons were
683 transfected into Huh7.5[C][E1E2][NS2]J6 by electroporation. B) Cells were fixed 48 h post
684 transfection and immunofluorescence analysis by staining for α -HA and DAPI was performed.
685 Shown are the respective merge pictures with the cell nuclei in blue and the α -HA staining in
686 green. Pictures were taken with a 100x magnification lens. D) Jc1 $\Delta p7^{\text{half}}$ was co-transfected into
687 Huh-7.5 cells with *in vitro* transcribed bicistronic JFH-1 helper replicons encoding for a signal
688 peptide (sp) downstream of p7J6, p7H14, p7J6-loop-H14, p7J6-C-ter-H14 and p7J6-loop-C-
689 terH14 in the first cistron as well as a G-Luc, respectively. E) Viral titers in supernatants 48 h
690 post transfection were determined by TCID₅₀ and the mean of three independent experiments is
691 depicted as $\log_{10}\text{TCID}_{50} + \text{SD}$.

692

693 **Figure 6**

694 **Characterization of HCV/NPHV p7 chimeras in recombinant HCV cell culture viruses.** A)

695 The p7 sequence from the HCV isolate J6 and the NPHV isolate H14 as well as the designated
696 chimeras were cloned into Jc1 or Jc1 HAHA-L-p7 as depicted. B) *In vitro* transcripts of the Jc1
697 HAHA-L-p7 constructs as well as Jc1 wildtype were transfected into Huh-7.5 cells and the
698 expression of HAHA-tagged p7 in cell lysates was visualized by Western blot analysis 48 h post
699 transfection. Additionally, the viral protein NS5A and the cellular protein β -actin were stained.

700 C) Expression of NS2 and E2 in lysates of cells transfected with *in vitro* transcripts of the Jc1

701 HAHA-L-p7 constructs was visualized 48 h post transfection by Western blot analysis. D) Viral
702 titers of the Jc1 p7 constructs were determined in supernatants 24 h, 48 h and 72 h after
703 transfection into Huh-7.5 cells. Shown are $\log_{10}\text{TCID}_{50}/\text{ml}$ as mean values of three independent
704 experiments + SD. E) Intra- and extracellular core amounts were measured 48 h post transfection
705 of the Jc1 p7 constructs into Huh-7.5 cells. The background level of extracellular core amounts
706 was set to the upper value of Jc1 p7H14, since this construct does not produce any infectious
707 particles. Two independent experiments were performed and the mean values +SD as \log_{10} core
708 fmol/l are shown. F) The specific infectivity was calculated based on viral titers in panel C and
709 extracellular core release in panel D.

710

711 **Figure 7**

712 **Effect of p7 inhibitors on infectivity of HCV/NPHV p7 chimeras.** *In vitro* transcripts of Jc1,
713 Jc1 p7J6-loop-H14 and Jc1 p7J6-C-ter-H14 were electroporated into Huh-7.5 cells. 4 h post
714 transfection the respective drug in two different concentrations or DMSO was added. Percentage
715 of infectivity was calculated by determining the viral titer by TCID_{50} and normalizing to the
716 DMSO control. Three independent experiments were performed. Test of the inhibitory effect of
717 A) Rimantadine (50 μM , 100 μM), B) NN-DGJ (5 μM , 50 μM) and C) NN-DNJ (5 μM , 50 μM].

718

719 **Funding information**

720 S. W. was supported by a stipend from the Helmholtz Centre for Infection Research and
721 supported by Hannover Biomedical Research School (HBRS) and the Centre for Infection
722 Biology (ZIB). E. S. was supported by the DFG (STE 1954/1-1) and intramural young
723 investigator award of the Helmholtz Centre for Infection Research. A.K. and N.Z. are supported
724 by the Oxford Glycobiology Institute. F.P. was supported by the Mapping project (ANR-11-
725 BINF-003) and the French agency ANRS. T. P. was supported by a grant from the Helmholtz
726 Association (SO-024) and by a grant from the European Research Council (ERC-2011-
727 StG_281473-VIRAFRONT).

728

729 **Acknowledgements**

730 We are grateful to Takaji Wakita for gift of the JFH1 isolate, to Jens Bukh for the J6CF strain, to
731 Charles Rice for Huh7.5 cells, the 9E10 and 6H6 monoclonal antibodies, to Ralf Bartenschlager
732 for the NS3-specific antibody, to Steven Fong for the E2-specific antibodies and to Genentech
733 and Arvind Patel for providing the AP33 antibody. We thank Daniel Todt for the statistical
734 analysis and all members of the Institute of Experimental Virology, Twincore, for helpful
735 suggestions and discussions.

736

737 **References**

- 738 1. **Kapoor A, Simmonds P, Gerold G, Qaisar N, Jain K, Henriquez JA, Firth C,**
739 **Hirschberg DL, Rice CM, Shields S, Lipkin WI.** 2011. Characterization of a canine
740 homolog of hepatitis C virus. *Proceedings of the National Academy of Sciences of the*
741 *United States of America* **108**:11608-11613.
- 742 2. **Burbelo PD, Dubovi EJ, Simmonds P, Medina JL, Henriquez JA, Mishra N, Wagner**
743 **J, Tokarz R, Cullen JM, Iadarola MJ, Rice CM, Lipkin WI, Kapoor A.** 2012.
744 Serology-enabled discovery of genetically diverse hepaciviruses in a new host. *Journal of*
745 *virology* **86**:6171-6178.
- 746 3. **Drexler JF, Corman VM, Muller MA, Lukashev AN, Gmyl A, Coutard B, Adam A,**
747 **Ritz D, Leijten LM, van Riel D, Kallies R, Klose SM, Gloza-Rausch F, Binger T,**
748 **Annan A, Adu-Sarkodie Y, Oppong S, Bourgarel M, Rupp D, Hoffmann B, Schlegel**
749 **M, Kummerer BM, Kruger DH, Schmidt-Chanasit J, Setien AA, Cottontail VM,**
750 **Hemachudha T, Wacharapluesadee S, Osterrieder K, Bartenschlager R, Matthee S,**
751 **Beer M, Kuiken T, Reusken C, Leroy EM, Ulrich RG, Drosten C.** 2013. Evidence for
752 novel hepaciviruses in rodents. *PLoS pathogens* **9**:e1003438.
- 753 4. **Quan PL, Firth C, Conte JM, Williams SH, Zambrana-Torrel CM, Anthony SJ,**
754 **Ellison JA, Gilbert AT, Kuzmin IV, Niezgoda M, Osinubi MO, Recuenco S,**
755 **Markotter W, Breiman RF, Kalemba L, Malekani J, Lindblade KA, Rostal MK,**
756 **Ojeda-Flores R, Suzan G, Davis LB, Blau DM, Ogunkoya AB, Alvarez Castillo DA,**
757 **Moran D, Ngam S, Akaibe D, Agwanda B, Briese T, Epstein JH, Daszak P,**
758 **Rupprecht CE, Holmes EC, Lipkin WI.** 2013. Bats are a major natural reservoir for
759 hepaciviruses and pegiviruses. *Proceedings of the National Academy of Sciences of the*
760 *United States of America* **110**:8194-8199.
- 761 5. **Kapoor A, Simmonds P, Scheel TK, Hjelle B, Cullen JM, Burbelo PD, Chauhan LV,**
762 **Duraisamy R, Sanchez Leon M, Jain K, Vandegrift KJ, Calisher CH, Rice CM,**
763 **Lipkin WI.** 2013. Identification of rodent homologs of hepatitis C virus and pegiviruses.
764 *mBio* **4**:e00216-00213.
- 765 6. **Lauck M, Sibley SD, Lara J, Purdy MA, Khudyakov Y, Hyeroba D, Tumukunde A,**
766 **Weny G, Switzer WM, Chapman CA, Hughes AL, Friedrich TC, O'Connor DH,**
767 **Goldberg TL.** 2013. A novel hepacivirus with an unusually long and intrinsically
768 disordered NS5A protein in a wild Old World primate. *Journal of virology* **87**:8971-8981.

- 769 7. **Firth C, Bhat M, Firth MA, Williams SH, Frye MJ, Simmonds P, Conte JM, Ng J,**
770 **Garcia J, Bhuva NP, Lee B, Che X, Quan PL, Lipkin WI.** 2014. Detection of zoonotic
771 pathogens and characterization of novel viruses carried by commensal *Rattus norvegicus*
772 in New York City. *mBio* **5**:e01933-01914.
- 773 8. **Corman VM, Grundhoff A, Baechlein C, Fischer N, Gmyl A, Wollny R, Dei D, Ritz**
774 **D, Binger T, Adankwah E, Marfo KS, Annison L, Annan A, Adu-Sarkodie Y,**
775 **Oppong S, Becher P, Drosten C, Drexler JF.** 2015. Highly divergent hepaciviruses
776 from African cattle. *Journal of virology* **89**:5876-5882.
- 777 9. **Baechlein C, Fischer N, Grundhoff A, Alawi M, Indenbirken D, Postel A, Baron AL,**
778 **Offinger J, Becker K, Beineke A, Rehage J, Becher P.** 2015. Identification of a Novel
779 Hepacivirus in Domestic Cattle from Germany. *Journal of virology* **89**:7007-7015.
- 780 10. **Scheel TK, Simmonds P, Kapoor A.** 2015. Surveying the global virome: identification
781 and characterization of HCV-related animal hepaciviruses. *Antiviral research* **115**:83-93.
- 782 11. **Pfaender S, Brown RJ, Pietschmann T, Steinmann E.** 2014. Natural reservoirs for
783 homologs of hepatitis C virus. *Emerging microbes & infections* **3**:e21.
- 784 12. **Global Burden of Disease Study C.** 2015. Global, regional, and national incidence,
785 prevalence, and years lived with disability for 301 acute and chronic diseases and injuries
786 in 188 countries, 1990-2013: a systematic analysis for the Global Burden of Disease
787 Study 2013. *Lancet* **386**:743-800.
- 788 13. **Hoofnagle JH.** 1997. Hepatitis C: the clinical spectrum of disease. *Hepatology* **26**:15S-
789 20S.
- 790 14. **Pawlotsky JM.** 2014. New hepatitis C therapies: the toolbox, strategies, and challenges.
791 *Gastroenterology* **146**:1176-1192.
- 792 15. **Bartenschlager R, Frese M, Pietschmann T.** 2004. Novel insights into hepatitis C virus
793 replication and persistence. *Advances in virus research* **63**:71-180.
- 794 16. **Scott C, Griffin S.** 2015. Viroporins: structure, function and potential as antiviral targets.
795 *The Journal of general virology* **96**:2000-2027.
- 796 17. **Carrere-Kremer S, Montpellier-Pala C, Cocquerel L, Wychowski C, Penin F,**
797 **Dubuisson J.** 2002. Subcellular localization and topology of the p7 polypeptide of
798 hepatitis C virus. *Journal of virology* **76**:3720-3730.
- 799 18. **Isherwood BJ, Patel AH.** 2005. Analysis of the processing and transmembrane topology
800 of the E2p7 protein of hepatitis C virus. *The Journal of general virology* **86**:667-676.

- 801 19. **Chandler DE, Penin F, Schulten K, Chipot C.** 2012. The p7 protein of hepatitis C virus
802 forms structurally plastic, minimalist ion channels. *PLoS computational biology*
803 **8**:e1002702.
- 804 20. **Luik P, Chew C, Aittoniemi J, Chang J, Wentworth P, Jr., Dwek RA, Biggin PC,**
805 **Venien-Bryan C, Zitzmann N.** 2009. The 3-dimensional structure of a hepatitis C virus
806 p7 ion channel by electron microscopy. *Proceedings of the National Academy of Sciences*
807 *of the United States of America* **106**:12712-12716.
- 808 21. **Griffin SD, Beales LP, Clarke DS, Worsfold O, Evans SD, Jaeger J, Harris MP,**
809 **Rowlands DJ.** 2003. The p7 protein of hepatitis C virus forms an ion channel that is
810 blocked by the antiviral drug, Amantadine. *FEBS letters* **535**:34-38.
- 811 22. **Clarke D, Griffin S, Beales L, Gelais CS, Burgess S, Harris M, Rowlands D.** 2006.
812 Evidence for the formation of a heptameric ion channel complex by the hepatitis C virus
813 p7 protein in vitro. *The Journal of biological chemistry* **281**:37057-37068.
- 814 23. **Montserret R, Saint N, Vanbelle C, Salvay AG, Simorre JP, Ebel C, Sapay N,**
815 **Renisio JG, Bockmann A, Steinmann E, Pietschmann T, Dubuisson J, Chipot C,**
816 **Penin F.** 2010. NMR structure and ion channel activity of the p7 protein from hepatitis C
817 virus. *The Journal of biological chemistry* **285**:31446-31461.
- 818 24. **Foster TL, Thompson GS, Kalverda AP, Kankanala J, Bentham M, Wetherill LF,**
819 **Thompson J, Barker AM, Clarke D, Noerenberg M, Pearson AR, Rowlands DJ,**
820 **Homans SW, Harris M, Foster R, Griffin S.** 2014. Structure-guided design affirms
821 inhibitors of hepatitis C virus p7 as a viable class of antivirals targeting virion release.
822 *Hepatology* **59**:408-422.
- 823 25. **Cook GA, Dawson LA, Tian Y, Opella SJ.** 2013. Three-dimensional structure and
824 interaction studies of hepatitis C virus p7 in 1,2-dihexanoyl-sn-glycero-3-phosphocholine
825 by solution nuclear magnetic resonance. *Biochemistry* **52**:5295-5303.
- 826 26. **OuYang B, Xie S, Berardi MJ, Zhao X, Dev J, Yu W, Sun B, Chou JJ.** 2013. Unusual
827 architecture of the p7 channel from hepatitis C virus. *Nature* **498**:521-525.
- 828 27. **Steinmann E, Penin F, Kallis S, Patel AH, Bartenschlager R, Pietschmann T.** 2007.
829 Hepatitis C virus p7 protein is crucial for assembly and release of infectious virions. *PLoS*
830 *pathogens* **3**:e103.

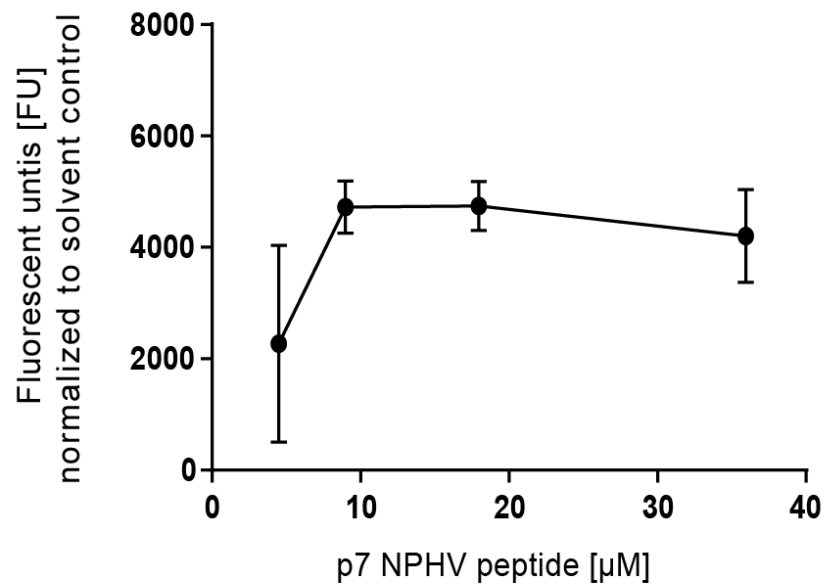
- 831 28. **Jones CT, Murray CL, Eastman DK, Tassello J, Rice CM.** 2007. Hepatitis C virus p7
832 and NS2 proteins are essential for production of infectious virus. *Journal of virology*
833 **81**:8374-8383.
- 834 29. **Madan V, Bartenschlager R.** 2015. Structural and Functional Properties of the Hepatitis
835 C Virus p7 Viroporin. *Viruses* **7**:4461-4481.
- 836 30. **Steinmann E, Pietschmann T.** 2010. Hepatitis C virus p7-a viroporin crucial for virus
837 assembly and an emerging target for antiviral therapy. *Viruses* **2**:2078-2095.
- 838 31. **Pfaender S, Cavalleri JM, Walter S, Doerrbecker J, Campana B, Brown RJ,**
839 **Burbelo PD, Postel A, Hahn K, Anggakusuma, Riebesehl N, Baumgartner W,**
840 **Becher P, Heim MH, Pietschmann T, Feige K, Steinmann E.** 2015. Clinical course of
841 infection and viral tissue tropism of hepatitis C virus-like nonprimate hepaciviruses in
842 horses. *Hepatology* **61**:447-459.
- 843 32. **Tanaka T, Kasai H, Yamashita A, Okuyama-Dobashi K, Yasumoto J, Maekawa S,**
844 **Enomoto N, Okamoto T, Matsuura Y, Morimatsu M, Manabe N, Ochiai K,**
845 **Yamashita K, Moriishi K.** 2014. Hallmarks of hepatitis C virus in equine hepacivirus.
846 *Journal of virology* **88**:13352-13366.
- 847 33. **Parera M, Martrus G, Franco S, Clotet B, Martinez MA.** 2012. Canine hepacivirus
848 NS3 serine protease can cleave the human adaptor proteins MAVS and TRIF. *PloS one*
849 **7**:e42481.
- 850 34. **Tamura K, Stecher G, Peterson D, Filipski A, Kumar S.** 2013. MEGA6: Molecular
851 Evolutionary Genetics Analysis version 6.0. *Molecular biology and evolution* **30**:2725-
852 2729.
- 853 35. **Thompson JD, Higgins DG, Gibson TJ.** 1994. CLUSTAL W: improving the sensitivity
854 of progressive multiple sequence alignment through sequence weighting, position-specific
855 gap penalties and weight matrix choice. *Nucleic acids research* **22**:4673-4680.
- 856 36. **Biasini M, Bienert S, Waterhouse A, Arnold K, Studer G, Schmidt T, Kiefer F,**
857 **Cassarino TG, Bertoni M, Bordoli L, Schwede T.** 2014. SWISS-MODEL: modelling
858 protein tertiary and quaternary structure using evolutionary information. *Nucleic acids*
859 *research* **42**:W252-258.
- 860 37. **Kalita MM, Griffin S, Chou JJ, Fischer WB.** 2015. Genotype-specific differences in
861 structural features of hepatitis C virus (HCV) p7 membrane protein. *Biochimica et*
862 *biophysica acta* **1848**:1383-1392.

- 863 38. **Humphrey W, Dalke A, Schulten K.** 1996. VMD: visual molecular dynamics. Journal
864 of molecular graphics **14**:33-38, 27-38.
- 865 39. **StGelais C, Tuthill TJ, Clarke DS, Rowlands DJ, Harris M, Griffin S.** 2007.
866 Inhibition of hepatitis C virus p7 membrane channels in a liposome-based assay system.
867 Antiviral research **76**:48-58.
- 868 40. **Steinmann E, Brohm C, Kallis S, Bartenschlager R, Pietschmann T.** 2008. Efficient
869 trans-encapsidation of hepatitis C virus RNAs into infectious virus-like particles. Journal
870 of virology **82**:7034-7046.
- 871 41. **Brohm C, Steinmann E, Friesland M, Lorenz IC, Patel A, Penin F, Bartenschlager
872 R, Pietschmann T.** 2009. Characterization of determinants important for hepatitis C virus
873 p7 function in morphogenesis by using trans-complementation. Journal of virology
874 **83**:11682-11693.
- 875 42. **Vieyres G, Brohm C, Friesland M, Gentsch J, Wolk B, Roingard P, Steinmann E,
876 Pietschmann T.** 2013. Subcellular localization and function of an epitope-tagged p7
877 viroporin in hepatitis C virus-producing cells. Journal of virology **87**:1664-1678.
- 878 43. **Pietschmann T, Kaul A, Koutsoudakis G, Shavinskaya A, Kallis S, Steinmann E,
879 Abid K, Negro F, Dreux M, Cosset FL, Bartenschlager R.** 2006. Construction and
880 characterization of infectious intragenotypic and intergenotypic hepatitis C virus
881 chimeras. Proceedings of the National Academy of Sciences of the United States of
882 America **103**:7408-7413.
- 883 44. **Appel N, Zayas M, Miller S, Krijnse-Locker J, Schaller T, Friebe P, Kallis S, Engel
884 U, Bartenschlager R.** 2008. Essential role of domain III of nonstructural protein 5A for
885 hepatitis C virus infectious particle assembly. PLoS pathogens **4**:e1000035.
- 886 45. **Keck ZY, Xia J, Wang Y, Wang W, Krey T, Prentoe J, Carlsen T, Li AY, Patel AH,
887 Lemon SM, Bukh J, Rey FA, Fong SK.** 2012. Human monoclonal antibodies to a
888 novel cluster of conformational epitopes on HCV E2 with resistance to neutralization
889 escape in a genotype 2a isolate. PLoS pathogens **8**:e1002653.
- 890 46. **Lindenbach BD, Evans MJ, Syder AJ, Wolk B, Tellinghuisen TL, Liu CC,
891 Maruyama T, Hynes RO, Burton DR, McKeating JA, Rice CM.** 2005. Complete
892 replication of hepatitis C virus in cell culture. Science **309**:623-626.

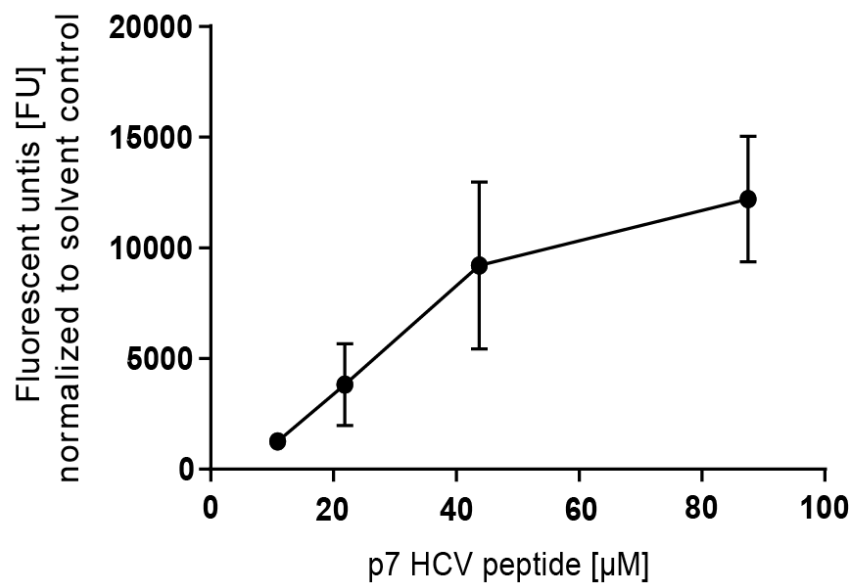
- 893 47. **Dentzer TG, Lorenz IC, Evans MJ, Rice CM.** 2009. Determinants of the hepatitis C
894 virus nonstructural protein 2 protease domain required for production of infectious virus.
895 *Journal of virology* **83**:12702-12713.
- 896 48. **Owsianka A, Tarr AW, Juttla VS, Lavillette D, Bartosch B, Cosset FL, Ball JK,**
897 **Patel AH.** 2005. Monoclonal antibody AP33 defines a broadly neutralizing epitope on the
898 hepatitis C virus E2 envelope glycoprotein. *Journal of virology* **79**:11095-11104.
- 899 49. **Altschul SF, Madden TL, Schaffer AA, Zhang J, Zhang Z, Miller W, Lipman DJ.**
900 1997. Gapped BLAST and PSI-BLAST: a new generation of protein database search
901 programs. *Nucleic acids research* **25**:3389-3402.
- 902 50. **Pearson WR.** 1991. Searching protein sequence libraries: comparison of the sensitivity
903 and selectivity of the Smith-Waterman and FASTA algorithms. *Genomics* **11**:635-650.
- 904 51. **Smith DB, Bukh J, Kuiken C, Muerhoff AS, Rice CM, Stapleton JT, Simmonds P.**
905 2014. Expanded classification of hepatitis C virus into 7 genotypes and 67 subtypes:
906 updated criteria and genotype assignment web resource. *Hepatology* **59**:318-327.
- 907 52. **Simmonds P, Bukh J, Combet C, Deleage G, Enomoto N, Feinstone S, Halfon P,**
908 **Inchauspe G, Kuiken C, Maertens G, Mizokami M, Murphy DG, Okamoto H,**
909 **Pawlotsky JM, Penin F, Sablon E, Shin IT, Stuyver LJ, Thiel HJ, Viazov S, Weiner**
910 **AJ, Widell A.** 2005. Consensus proposals for a unified system of nomenclature of
911 hepatitis C virus genotypes. *Hepatology* **42**:962-973.
- 912 53. **Nieva JL, Madan V, Carrasco L.** 2012. Viroporins: structure and biological functions.
913 *Nature reviews. Microbiology* **10**:563-574.
- 914 54. **Pavlovic D, Neville DC, Argaud O, Blumberg B, Dwek RA, Fischer WB, Zitzmann**
915 **N.** 2003. The hepatitis C virus p7 protein forms an ion channel that is inhibited by long-
916 alkyl-chain iminosugar derivatives. *Proceedings of the National Academy of Sciences of*
917 *the United States of America* **100**:6104-6108.
- 918 55. **Griffin S.** 2014. "Too little, too late?" Will inhibitors of the hepatitis C virus p7 ion
919 channel ever be used in the clinic? *Future medicinal chemistry* **6**:1893-1907.
- 920 56. **Carrere-Kremer S, Montpellier C, Lorenzo L, Brulin B, Cocquerel L, Belouzard S,**
921 **Penin F, Dubuisson J.** 2004. Regulation of hepatitis C virus polyprotein processing by
922 signal peptidase involves structural determinants at the p7 sequence junctions. *The*
923 *Journal of biological chemistry* **279**:41384-41392.

- 924 57. **Scull MA, Schneider WM, Flatley BR, Hayden R, Fung C, Jones CT, van de Belt M,**
925 **Penin F, Rice CM.** 2015. The N-terminal Helical Region of the Hepatitis C Virus p7 Ion
926 Channel Protein Is Critical for Infectious Virus Production. *PLoS pathogens*
927 **11:e1005297.**
- 928 58. **StGelais C, Foster TL, Verow M, Atkins E, Fishwick CW, Rowlands D, Harris M,**
929 **Griffin S.** 2009. Determinants of hepatitis C virus p7 ion channel function and drug
930 sensitivity identified in vitro. *Journal of virology* **83:7970-7981.**
- 931 59. **Sakai A, Claire MS, Faulk K, Govindarajan S, Emerson SU, Purcell RH, Bukh J.**
932 2003. The p7 polypeptide of hepatitis C virus is critical for infectivity and contains
933 functionally important genotype-specific sequences. *Proceedings of the National*
934 *Academy of Sciences of the United States of America* **100:11646-11651.**
- 935 60. **Steinmann E, Whitfield T, Kallis S, Dwek RA, Zitzmann N, Pietschmann T,**
936 **Bartenschlager R.** 2007. Antiviral effects of amantadine and iminosugar derivatives
937 against hepatitis C virus. *Hepatology* **46:330-338.**
- 938 61. **Crooks GE, Hon G, Chandonia JM, Brenner SE.** 2004. WebLogo: a sequence logo
939 generator. *Genome research* **14:1188-1190.**
- 940 62. **von Heijne G.** 1990. The signal peptide. *The Journal of membrane biology* **115:195-201.**
- 941 63. **von Heijne G.** 1998. Life and death of a signal peptide. *Nature* **396:111, 113.**
- 942

A)



B)



C)

